

Article

Carbon Nanotubes-Filled Siloxane Composite Foams for Oil Recovery Application: Compression Properties

Elpida Piperopoulos ^{1,*}, Luigi Calabrese ¹, Emanuela Mastronardo ², Edoardo Proverbio ¹
and Candida Milone ¹

¹ Department of Engineering, University of Messina, Contrada di Dio Sant'Agata, 98166 Messina, Italy; lcalabrese@unime.it (L.C.); eproverbio@unime.it (E.P.); cmilone@unime.it (C.M.)

² Institute of Catalysis and Petrochemistry, Spanish National Research Council (CSIC), C/Marie Curie, 2, E-28049 Madrid, Spain; e.mastronardo@csic.es

* Correspondence: epiperopoulos@unime.it; Tel.: +39-090-676-5558

Received: 15 May 2020; Accepted: 2 July 2020; Published: 10 July 2020



Abstract: This paper studies the correlation between oil recovery usability and mechanical behavior under compression loads of an innovative oil recovery material. The examined composites are silicone foams filled with carbon nanotubes (CNT). Here, the reutilization of oil recovery processes of the newly developed composite foams is evaluated. In this regard, static and cyclic compressive tests are carried out. Samples filled with pristine and functionalized CNT are tested to evaluate the influence of the filler's characteristics on the composite foam's mechanical behavior. The results show that the presence of CNT (CNT-0) increases the elastic modulus (0.030 MPa) and collapse stress (0.010 MPa) of the siloxane matrix. On the contrary, as the CNT functionalization degree increases, a worsening of the composite's mechanical performance is observed. CNT-0 foam evidences, also, the optimal mechanical stability to cyclic compressive loads, maintaining high stress values until 30 cycles. Furthermore, a correlation between the absorption capacity, elastic modulus, and cyclability is reported, highlighting a simplified approach to tailor the high absorption durability performance of filled CNT silicone foams. The promising results confirm the possible reuse of these new composite foams as absorbent materials for oil spill recovery applications.

Keywords: carbon nanotubes; composite foam; compression test; mechanical stability

1. Introduction

The Mediterranean Sea is a semi-closed basin; its water represents around 0.7% of the world's marine waters and it is an invaluable source of biodiversity. It contains 12,000 marine species, about 10% of the total animals that populate the planet's seas. Moreover, it acts as a human resource for maritime transport, the tourist industry, etc. As regards maritime traffic, approximately 200,000 large vessels operate annually in the Mediterranean Sea, including ferries, cargo, and commercial vessels, of which around 300 daily tankers carry petroleum products. Over 350 million tons per year pass through its basin (over 25% of the world quantity). Every year, the Mediterranean Sea suffers oil spills of about 600,000 tons. Lastly, 27 accidents occurred in the last 30 years, for a total of about 272,000 tons of spilled oil [1]. For these events, which are extremely harmful to the marine environment, all the involuntary spills of hydrocarbons and so-called "operational activities" must be taken into account. This leads to a seriously compromised ecosystem with environmental damage that is difficult to estimate even by current scientific investigation systems [2,3]. The articulated system of global maritime transport in recent decades led the international community to adopt more stringent rules to guarantee the better

environmental safety of transports and the scientific research community to develop more efficient oil spill recovery systems aiming at an almost full recovery of the released oil [4–6]. Older techniques such as dispersion [7] or in situ burning [8] have been supplanted with more efficient methodologies that can leave no residues and speed up the intervention. In this regard, the development of highly efficient absorbent materials capable of recovering the spilled oil is widely investigated [9–12]. Absorbent materials are considered to be of interest in hydrocarbon spill recovery for their high oleophilicity and hydrophobicity [8]. The aim is to convert polluting liquid into a semi-solid material to be disposed of more easily and safely [13]. The efficient use of absorbent materials is assessed by factors such as absorption capacity and absorption rate. Among absorbent systems, foams are a new research frontier with promising results. In fact, the macroporous structure acts as a container for spilled oil in recovery phase, thus allowing significant absorption percentages due to the free volume that can be filled by the contaminant [14–16]. Ko et al. [17] reported a polydimethylsiloxane (PDMS) sponge coated with a superhydrophobic molybdenum disulfide (MoS_2) layer, establishing its excellent superhydrophobicity and high oil absorption (>97 wt.%). Wang et al. [18] presented a facile and low-cost approach for fabricating magnetic, durable, and superhydrophobic carbon sponges. Carbon sponges can controllably and selectively adsorb oils from oil-water mixtures up to almost 27 wt.% in gasoline. Li et al. [19] modified Fe_3O_4 nanoparticles with silane compounds (tetraethoxysilane and trimethoxy (heptadecafluorodecyl)silane) to obtain nanoparticles with magnetic capabilities. These particles were used to obtain, by a drop-coating method, a superhydrophobic surface on several substrates, such as PU sponge, cotton fabric, and filter paper. These sponges showed a high absorption capability on natural or artificial oil (40.3, 39.3, and 46.3 g g^{-1} , in peanut oil, pump oil, and silicone oil, respectively). Furthermore, a crucial factor for absorption material application in oil recovery is its reusability. Indeed, the possibility of using absorbent materials for numerous cycles further increases their sustainability. Additionally, they are beneficial in terms of cost-effectiveness for the process and permit the user to minimize the problems of handling recovered oils and the related product disposal at the end of their use.

Yuan et al. [20] synthesized sponges with high hydrophobicity, recyclability, and absorption capacities (up to 32.26 g in oil and 52.51 g g^{-1} in organic solvents). They were produced using low-cost raw materials and by the unidirectional freeze-casting technique. After regeneration, the sponges can be reused more than five times without losing their efficiency. Ding et al. [21] realized oil absorbents containing β -Cyclodextrin moieties that showed an excellent oil absorbency (79.1 g g^{-1} in CCl_4 , 72.8 g g^{-1} in CHCl_3 , 43.7 g g^{-1} in xylene, and 45.7 g g^{-1} in toluene). Absorbents can be used at least six times. Korhonen et al. [22] prepared hydrophobic nanocellulose aerogels as recyclable oil absorbents that are able to be reused after washing, recycled, or incinerated with the absorbed oil. Cellulose is a renewable material and titanium dioxide is environmentally safe, thus endorsing their possible use in environmental-based application fields. In the authors' previous works, carbon nanotube-based silicone foams were investigated. Their absorption capacity [23] and absorption kinetic [24] were assessed. The produced composites showed a good reusability for up to 10 absorption and mechanical compressive squeezing cycles. The good mechanical stability of the composite foam plays a relevant role on the foam reusability, allowing an effective and reliable absorption capacity during its cyclic reuse. Therefore, determining the correlation between the mechanical and adsorption properties could give added value to the performance assessment.

In this regard, the aim of this work is to examine the mechanical compression behavior of previously developed foams. The promising absorption performance and high cyclability of the composite materials are correlated with their morphological properties and mechanical stability. The result of a close correlation between these characteristics leads to a definition of guiding parameters for designing highly efficient foam, directing the synthesis procedure, and ensuring material durability in oil recovery applications. The main goal is defining an optimum design of the carbon nanotubes (CNT)-silicone composite foam to have a suitable mechanical resistance to bear the stresses induced by the absorption of oil pollutants. The synthesis of a highly cycling absorbent material allows one to

simplify and reduce the management costs of the oil recovery procedure, allowing an easier life and cost assessment of the process with respect to other products generally used in this context [25].

2. Materials and Methods

2.1. Filler Synthesis

Pure and functionalized carbon nanotubes (CNT) were synthesized as previously reported in the literature [23]. The used procedure is schematized in Figure 1. Synthesis was carried out in a chemical vapor deposition (CVD) apparatus in a 120 cc/min flow (1:1 $i\text{-C}_4\text{H}_{10}:\text{H}_2$). After synthesis, the obtained products were purified with a 1 M solution of NaOH at 80 °C and a subsequent treatment in a 37 wt.% HCl solution at room temperature [26]. The produced Multi-Walled Carbon Nanotubes (MWCNT) had an average external diameter of 14 nm and a surface area of 190 m^2/g , as measured by Brunauer – Emmett – Teller (BET) analysis. Then, the CNT were functionalized by nitric acid vapors [27]. Functionalized CNT are considered because the large amount of carboxyl groups on their surface could generate an acceptable chemical affinity between the matrix and the filler, ensuring a good mechanical stability and even increasing the filler percentage [23].

The functionalization degree of the CNT was determined by means of thermogravimetric technique, as reported elsewhere [23].

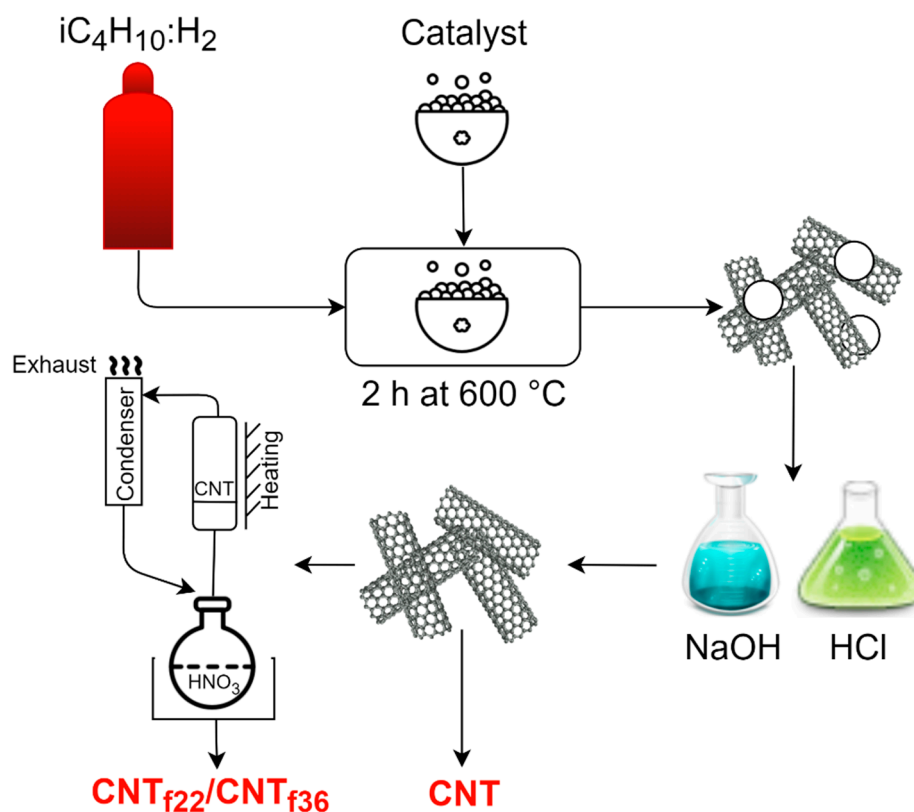


Figure 1. Filler synthesis procedure.

2.2. Foam Synthesis

Commercially available silicone foam reactants were acquired by Gelest Inc. (Morrisville, PA, USA) without any commercial filler. Poly (dimethylsiloxane-co-methylhydrosiloxane), trimethylsilyl-terminated PMHS (M.W. 5500-6500 CAS: 68037-59-2), and silanol-terminated polydimethylsiloxane PDMS (M.W. 110,000 CAS: 70131-67-8) compounds were used as reactants for the foam synthesis. Tin(II) 2-ethylhexanoate (Sn(II)) (d:1.12, M.W. 405.11, 50%, CAS. 301-10-0), purchased by Aldrich Chemical (Saint Louis, MO, USA) was used as a catalyst. In particular, foam preparation was carried out

according to the procedure shown in Figure 2. The CNT (0.250 g) were spread in ethanol (2 mL) for 5 min in an ultrasonic bath and left overnight under constant magnetic stirring. Then, the mixture was dispersed in PDMS (2 g) under high shear mixing for about 60 s. After that, the PMHS (1 g) was added with a siloxane PDMS/PMHS weight ratio 2:1 vigorously stirring for 15 s. The solvents, water (0.5 g), and ethanol (0.2 g), were used to reduce the composite slurry viscosity. Lastly, a tin catalyst (0.5 g) was added while stirring for about 15 s. The final mixture was put in a cylindrical mold with diameter 2 cm and put in an oven at 60 °C for 24 h. Foaming is caused by the chemical reaction between PDMS and PMHS described elsewhere [24,28]. The filler content is 5.6 wt.% in all the produced foams.

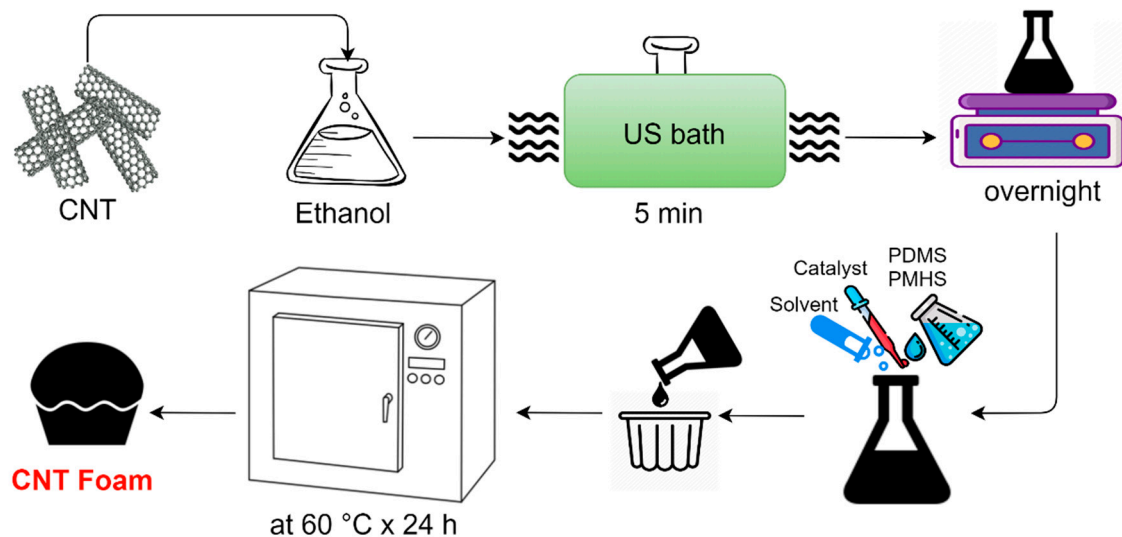


Figure 2. Foam synthesis procedure.

Table 1 shows all the produced formulations with the codified products and filler functionalization degree. The composite foam batches were codified based on a prefix “CNT-” and a number indicating the degree of functionalization of the CNT filler. CNT-0 designates a composite foam filled with pristine CNT. CNT-22 and CNT-36 indicate composite foams filled with CNT functionalized at 22 wt.% and 36 wt.%, respectively. As a reference, an unfilled silicone foam (SF-0) was also considered.

The foam morphology was evaluated by a scanning electron microscope (FEI Quanta FEG 450) operating at 5.00 kV. The foam bulk (apparent) density was calculated from the weight to volume ratio. Five measurements were taken for each kind of foam.

Table 1. Composite solution compositions (carbon nanotubes (CNT): pristine; CNT_{f22}: degree of functionalization 22 wt.%; CNT_{f36}: degree of functionalization 36 wt.%).

Code	PDMS	PMHS	Ethanol	Water	Sn(II)	CNT	CNT _{f36}	CNT _{f36}
	(wt.%)	(wt.%)	(wt.%)	(wt.%)	(wt.%)	(wt.%)	(wt.%)	(wt.%)
	Siloxane	Siloxane	Solvent	Solvent	Catalyst	Filler	Filler	Filler
SF-0	47.6	23.8	4.8	11.9	11.9	0.0	0.0	0.0
CNT-0	45.0	22.5	4.5	11.2	11.2	5.6	0.0	0.0
CNT-22	45.0	22.5	4.5	11.2	11.2	0.0	5.6	0.0
CNT-36	45.0	22.5	4.5	11.2	11.2	0.0	0.0	5.6

2.3. Absorption Test

An absorption test was conducted to determine the absorption capacity of the composite foams. Four common oils (kerosene, naphtha, crude, and pump oils) were selected for the absorption experiments. As reported elsewhere [23,24,29], each composite foam (1 cm³ of volume) was put in a 250 mL beaker filled with the selected oil at room temperature and under mild stirring. After absorption,

the foam was left to rest for 30 s to expel the easily released liquid and then weighted. The absorption capacity was calculated as Equation (1).

$$\text{Absorption capacity (wt.\%)} = \frac{m_t - m_0}{m_0}, \quad (1)$$

where m_t (g) is the sample mass after t sorption time and m_0 (g) is the sample initial mass. The saturation absorption capacity is defined when the absorption capacity does not change with time. Each experiment was carried out three times to confirm the test repeatability. The samples, after the absorption test, were mechanically regenerated by five simple manual squeezings and reimmersed until complete saturation in oil. The same procedure was carried out for ten sorption-squeezing cycles in order to evaluate the reusability of the prepared foams [23].

2.4. Compression Tests

Cubic test specimens ($10 \times 10 \times 10 \text{ mm}^3$), were obtained by cylindrical-shaped samples. A universal testing machine (2.5 kN Zwick Line) equipped with a 2.5 kN load-cell (sensitivity of 0.001 N) was used to carry out static and cyclic compressive tests at room temperature. The crosshead speed was 1.0 mm/min. A multipurpose WD 40 oil was used to lubricate the compression plates in order to reduce the friction of the samples with the plates. A static compression test up to densification was performed for each investigated composite foam. Moreover, 30 cyclic compression tests up to 50% strain were carried out for all the batches.

3. Results and Discussion

3.1. Absorbent Properties and Reuse

Preliminarily, each composite foam was tested to determine its absorption ability. Figure 3 shows the absorption capacity for each investigated foam at varying pollutants. A striking observation is that all the samples present higher absorption values for light oils (kerosene and naphtha) and lower ones for heavy oils (crude oil and pump oil). This behavior has been widely discussed in previous works [23] and is due to the different dynamic viscosity of the investigated oils. Light oils, like kerosene and naphtha, present a low dynamic viscosity, contrary to heavy oils. When the dynamic viscosity is higher, the fluid reluctance to deformation is also high, and thus the heavy oil entry into the foam pores is obstructed. In particular, the SF-0 and CNT-0 samples exhibit a similar behavior in heavy oil, reaching an absorption capacity in pump oil and crude oil of about 119 wt.% and 140 wt.%, respectively. Instead, in light oils an increase in the absorption capacity is recorded for the CNT-0 sample compared to SF-0. In particular, a 25 wt.% increase is verified in kerosene oil and a 10 wt.% increase in naphtha. On the contrary, a global reduction in terms of the absorption capacity values is noticed when functionalized CNT are used as fillers. In particular, in kerosene and naphtha oils, the CNT-22 and CNT-36 batches achieve 401 wt.% and 540 wt.% and 458 and 490 wt.%, respectively. Furthermore, the most important purpose of research on innovative absorbent materials for oil recovery is, undoubtedly, the reuse of such materials. This entails a substantial decrease in terms of material costs and their subsequent disposal, since their long life cycle avoids the repeated use of ever-new material and slows down their conveyance towards disposal procedures. To this purpose, absorbent material must have the ability to be used several times without losing its absorbent properties, rather keeping them for long cycles of use and without being damaged. Hence, the cyclability of the developed composite materials was investigated here.

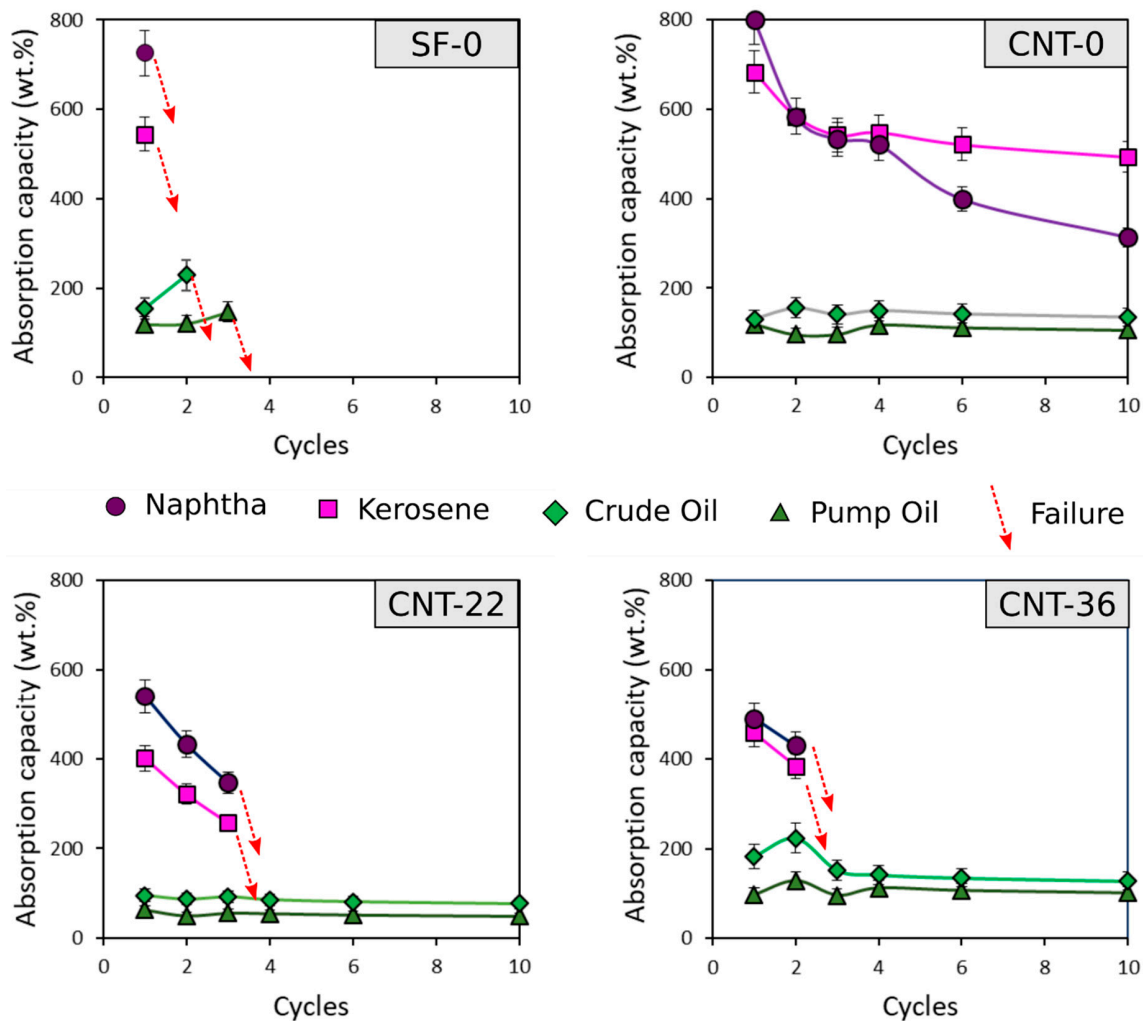


Figure 3. Absorption capacity up to 10 cycles for each investigated foam.

Figure 3 shows the absorbent behavior of each foam during 10 use cycles in each tested oil, unless the material is damaged by fracture (red arrows in Figure 3) and cannot be re-used in the next cycle. Comparing CNT-0 with the SF-0 sample, although the sorbing capacity of the material is quite similar, a totally different behavior is observed as the absorption cycles increase. Indeed, the use of CNT as a filler enhances the silicone foam structural stability, and the sample is not damaged until the tenth cycle. On the contrary, the SF-0 foam resists for a few cycles in heavy oils and only for one cycle in kerosene and naphtha. In addition, the CNT-0 foam in light oils loses 55 wt.% of its absorbent performance during cycling, thus indicating a cycle threshold over which the oil spill recovery capabilities of the CNT-based foam are negligible. On the contrary, in pump oil and crude oil it maintains an almost stable saturated absorption capacity. This is due to the high volume of increase in light oils that is not found in the heavy oils case. In fact, this foam expansion, due to the large amount of absorbed pollutant and the repeated subsequent compression during oil release, generates cracks and deformations in the foam matrix which are the cause of the consistent efficiency loss. Functionalized CNT fillers improve the reuse behavior compared to SF-0, but they worsen the mechanical properties of CNT-0 foam. In fact, failure in kerosene and naphtha oils occurs after the third and the second cycles for CNT-22 and CNT-36, respectively, concluding that the higher the degree of functionalization, the worse the structural stability. Moreover, it is worth noting that for all investigated foams the reusability is lacking in light oils recovery, in which the sorption capacity is considerable compared with other pollutant oil. Consequently, higher mechanical stresses take place in sorption/squeezing cycles, due to the relevant foam volume increase during the high oil absorption [23].

3.2. Morphological Analysis

Since, as is already known and described elsewhere [30], a material's performance is closely related to its morphological properties, to better understand the composite foam's behavior in oil recovery applications, a morphological analysis was conducted. Cross sections along the foaming direction of the realized foams were graphically processed by digital image analysis to view the macroporosity distribution and to calculate the mean pore diameter (Figure 4).

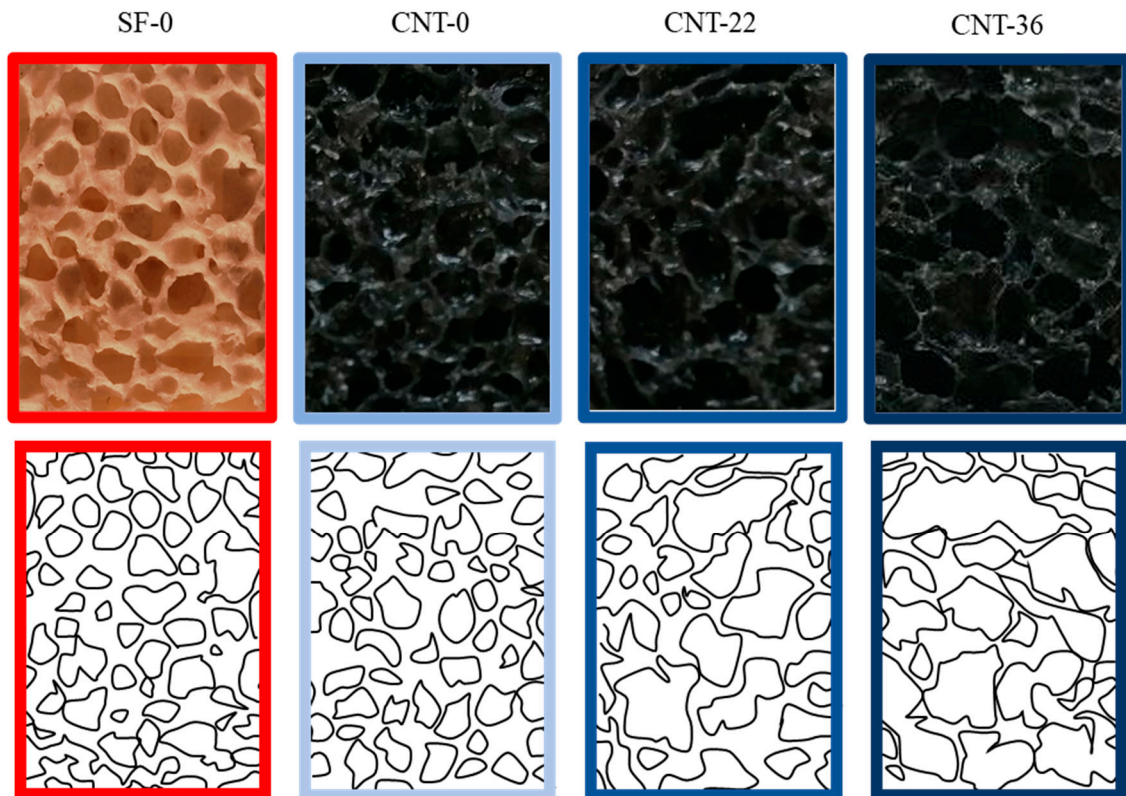


Figure 4. Cross section images along the foaming direction of the composite foams and the digital image processing of their macroporosity.

Unfilled silicone foam (SF-0) shows a quite isotropic and regular structure of mostly spheroidal cells with interconnected pores (Figure 4). Moreover, some heterogeneities of bubble size can be evidenced. At the foam base, some elongated bubbles are clearly identified. Comparing CNT-0 foam with the unfilled one, the pore size appears smaller and the pore distribution more regular. The cell walls are thick enough to guarantee an effective mechanical stability. As reported in [31], the filler addition in the silicone matrix increases the composite slurry viscosity and the nucleating effect during foam preparation, with a subsequent decrease in pore size. On the contrary, the higher reactivity of functionalized CNT increases their interaction with the silicone matrix, promoting physical and chemical bubbling during the foaming process and thus causing the formation of larger pores [23] (Figure 4).

Furthermore, this latter phenomenon is more sensitive when using functionalized CNT fillers. CNT filler has a large amount of reactive groups on its surface that are able to chemically react with the siloxane matrix [23], increasing the interfacial filler/matrix stiffness and decreasing the foam flexibility. The larger bubble growth when using functionalized CNT induces a larger amount of defects such as voids and microcracks which are easily visible with an SEM microscope, especially in the CNT-36 sample (red arrows in Figure 5d). Meanwhile, the CNT-0 foam structure (Figure 5b) is characterized by uniform cellular walls without evident cracks, indicating a more stable foaming process compared to the functionalized one.

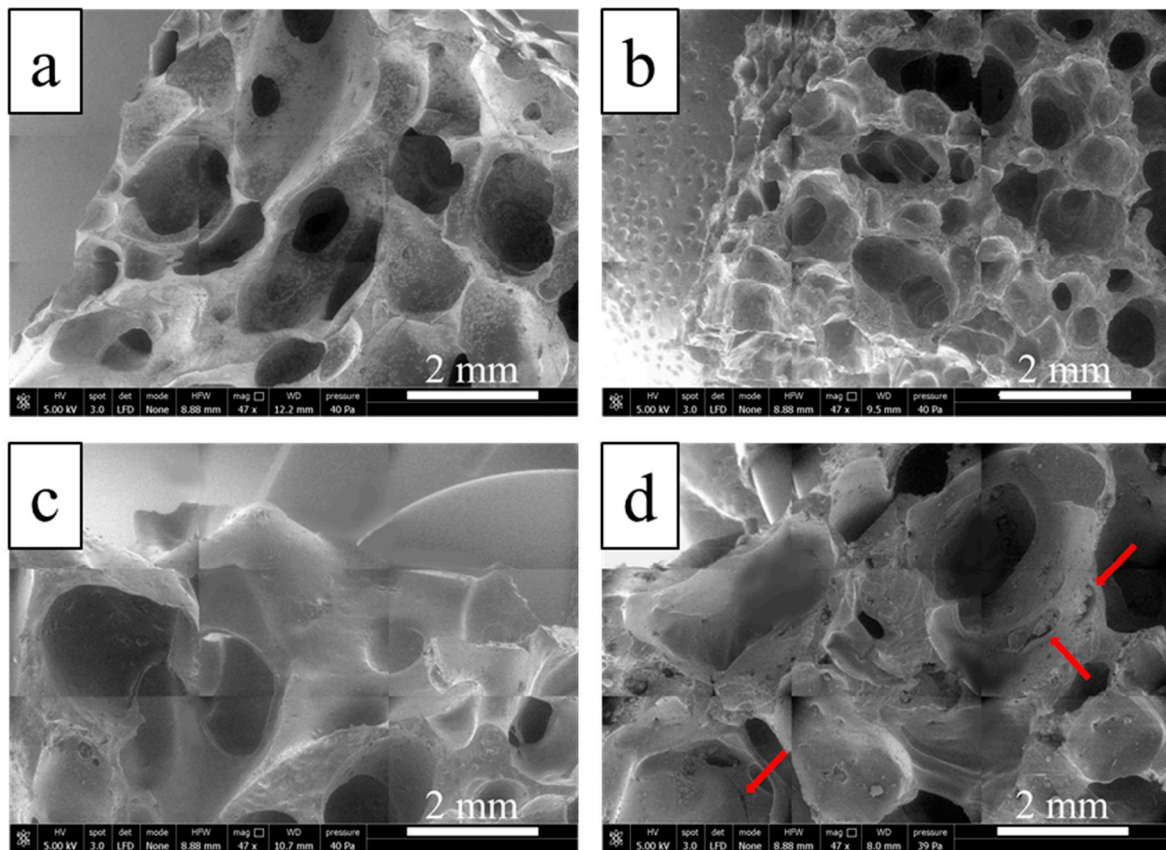


Figure 5. SEM micrographs of composite foams: (a) SF-0, (b) CNT-0, (c) CNT-22, (d) CNT-36.

From the SEM analysis (Figure 5), the mean pore size was confirmed as the pore's mean equivalent diameter by ImageJ software on 10 SEM images for each sample and corrected according to the Schwartz–Saltykov method (see Table 2). SF-0 presents a pore size value of 1.75 mm, higher than the CNT-0 sample's one (1.05 mm). Moreover, the results confirmed a pore size increase for functionalized CNT-filled foams (1.82 and 2.00 mm, respectively, for CNT-22 and CNT-36). As a consequence, the higher the mean pore size, the lower the foam apparent density (Table 2). In fact, the density of CNT-0 was calculated as 0.315 g/cm^3 , higher than the unfilled foam (0.280 g/cm^3) and CNT-22 and CNT-36—respectively, 0.253 and 0.251 g/cm^3 .

Table 2. CNT-silicone composite foams structural properties and compressive parameters: elastic modulus, collapse stress, densification strain, apparent density, and pore size.

Code	Elastic Modulus [MPa]	Collapse Stress [MPa] (40% Strain)	Densification Strain [%]	Apparent Density [g/cm^3]	Pore Size (mm)
SF-0	0.017 ± 0.003	$0.005 \pm 3 \times 10^{-4}$	69.18 ± 2.34	0.280 ± 0.015	1.75 ± 0.005
CNT-0	0.030 ± 0.005	$0.010 \pm 2 \times 10^{-4}$	68.08 ± 1.52	0.315 ± 0.023	1.05 ± 0.002
CNT-22	0.022 ± 0.010	$0.005 \pm 4 \times 10^{-3}$	69.15 ± 3.32	0.253 ± 0.078	1.82 ± 0.010
CNT-36	0.006 ± 0.012	$0.002 \pm 8 \times 10^{-3}$	70.21 ± 3.65	0.251 ± 0.089	2.00 ± 0.008

3.3. Static Compression Test

In Figure 6, the evolution of the stress (principal axis) and tangent modulus (secondary axis) is plotted as a function of strain for a reference silicone foam (elastic modulus in the secondary axis). The tangent modulus is a useful parameter to study materials that follow a non-linear elastic behavior. Indeed, its value and trend is helpful for estimating the variation in deformation for a specific stress range [32]. Silicone foams have a non-linear compression behavior. As reported in Figure 6, the initial trend can be associated with the initial stabilization phase. This curve section is typically fairly noisy and it is not indicative of the foam mechanical behavior and can be avoided. After that, three different steps (codified as regimes) can be identified:

- I. At a low stress level, an elastic Hookean regime, recognized by a rather linear correlation between stress and strain, can be detected. The curve slope of this area identifies Young's modulus (E) of the foam. The structure of the foam is slightly deformed, but it can still be considered structurally stable. Stresses transferred between the bubble walls are not so high as to bring structural cellular alterations. In the elastic regime, the linear behavior depends on the wall bending or stretching for the open or closed bubbles, respectively [33]. In this region, observing the modulus trend a peak at about a strain of 15% is observed. Afterward, a gradual decrease takes place that indicates the triggering of a progressive mechanical instability state anticipating the evolution of the elastic regime towards the subsequent collapse regime.
- II. At an intermediate strain, the stress value reaches a local stabilization. In this stage, a large stress collapse takes place due to the wall collapse of the foam pores. This leads to progressively decreasing the modulus. This dependence is closely linked to the relationship between stress and strain in the collapse regime. The more constant the tendency to stress, the lower the modulus value. The plateau is associated with cell collapse. There are a number of local collapses that run through the structure in the presence of a critical stress, leading to a high deformation throughout the material with no relevant change in the stress magnitude [34]. This area is influenced by the elastic or elastoplastic behavior of the foam. In particular, for an elastic foam the plateau is due to elastic deformation, while in elastoplastic foams it is due to the creation of plastic areas [33]. Therefore, based on the mechanical compression behavior of the macroporous material [35], the plateau region can be sloping, flat, or slightly increasing [36].
- III. When the cell collapse is almost complete, the cell walls begin to interact together so that a rapid increase in stress occurs as the compression tension increases. At the same time, a sharp increase in the modulus is observed. This last part of the curve is called the "densification" regime. Foamed materials with a large compressibility, as reported in Figure 6, are characterized by very high densification strain.

As reported in Figure 7, the presence of the filler significantly influences the mechanical behavior of the composite foams. The composite CNT-0 foam reaches a high stress value during the collapse regime, showing a large amount of absorbed specific energy. Energy is dissipated through the deformation, instability, and fracture of cells. During the plateau phase, which is extended up to large deformations, the foam endures significant compression strains and consequently absorbs a large specific energy [37]. During this process, the cells edges collapse by elastic deformation, whereas the cell faces bend and the walls collapse by folding [38].

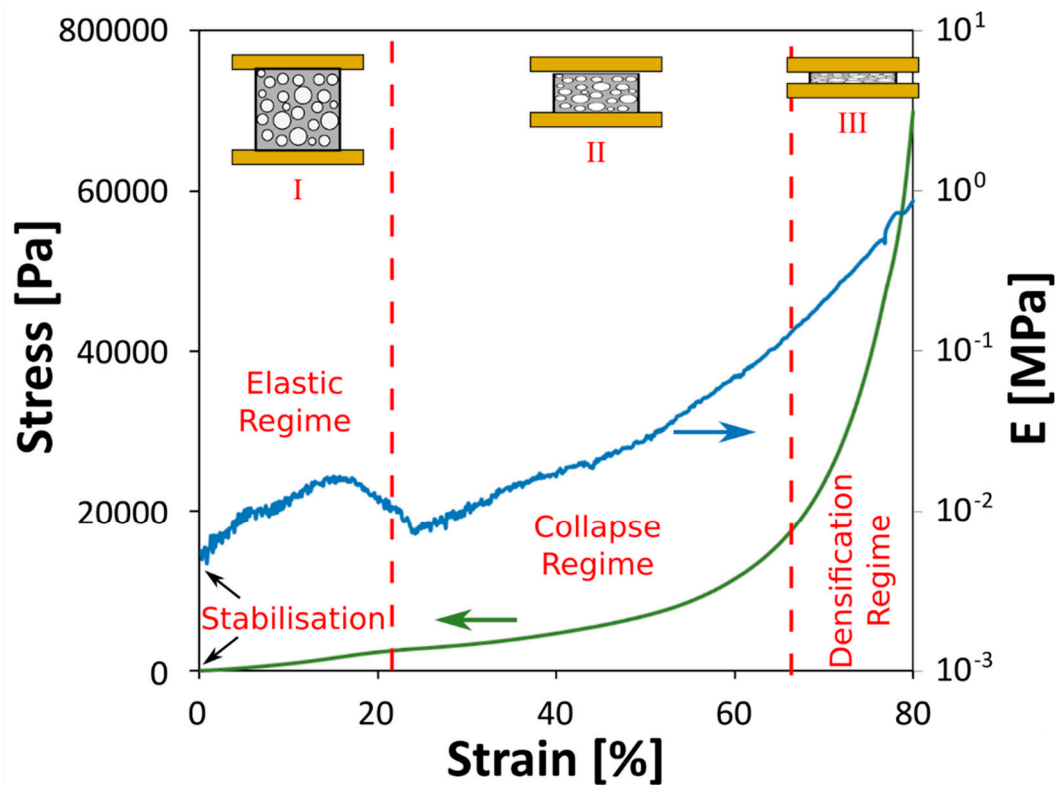


Figure 6. Stress–strain primary axis and modulus–strain secondary axis curves of a composite foam.

CNT-filled foam (CNT-0) presents an initial slope (better highlighted in the magnification plot reported in Figure 7b) related to the foam elasticity regime that is higher than SF-0. However, using functionalized CNT this effect disappears, especially in the case of the CNT-36 sample, whose slope decreases until it becomes lower than the SF-0 one, while the CNT-22 approximates it. In particular, for CNT-0 a modulus of about $E_{\text{CNT-0}} = 0.030$ MPa is observed and lower values are detected for the remaining foam batches: $E_{\text{SF-0}} = 0.017$ MPa, $E_{\text{CNT-22}} = 0.022$ MPa, and $E_{\text{CNT-36}} = 0.006$ MPa (Table 2). All the samples show a densification zone at high strain values, confirming a good compressibility and settling their potential applicability for oil spill reuse.

Further information can be acquired evaluating also the collapse stress. It increases using unfunctionalized CNT as a foam filler (0.01 MPa). Furthermore, functionalized CNT penalizes the foam structure, reaching the same value as the SF-0 foam for the CNT-22 sample (0.005 MPa) and especially significantly worsening the behavior of the CNT-36 foam (0.002 MPa). A stiffness increase is observable in the CNT-0 batch. This is generally associated with a decrease in the final deformation. Furthermore, locally, at lower strain values, an evolution from the elastic regime to the collapse one occurs. Moreover, the collapse stress increases. This behavior is due either to the homogenous and regular foam structure and to the presence of the filler, which acts as a rigid element in a flexible matrix. Therefore, the stress required to cause the collapse by cell wall buckling is larger for the filled foam. However, this is not observable in foams filled with functionalized CNT, hence their mechanical behavior is completely different.

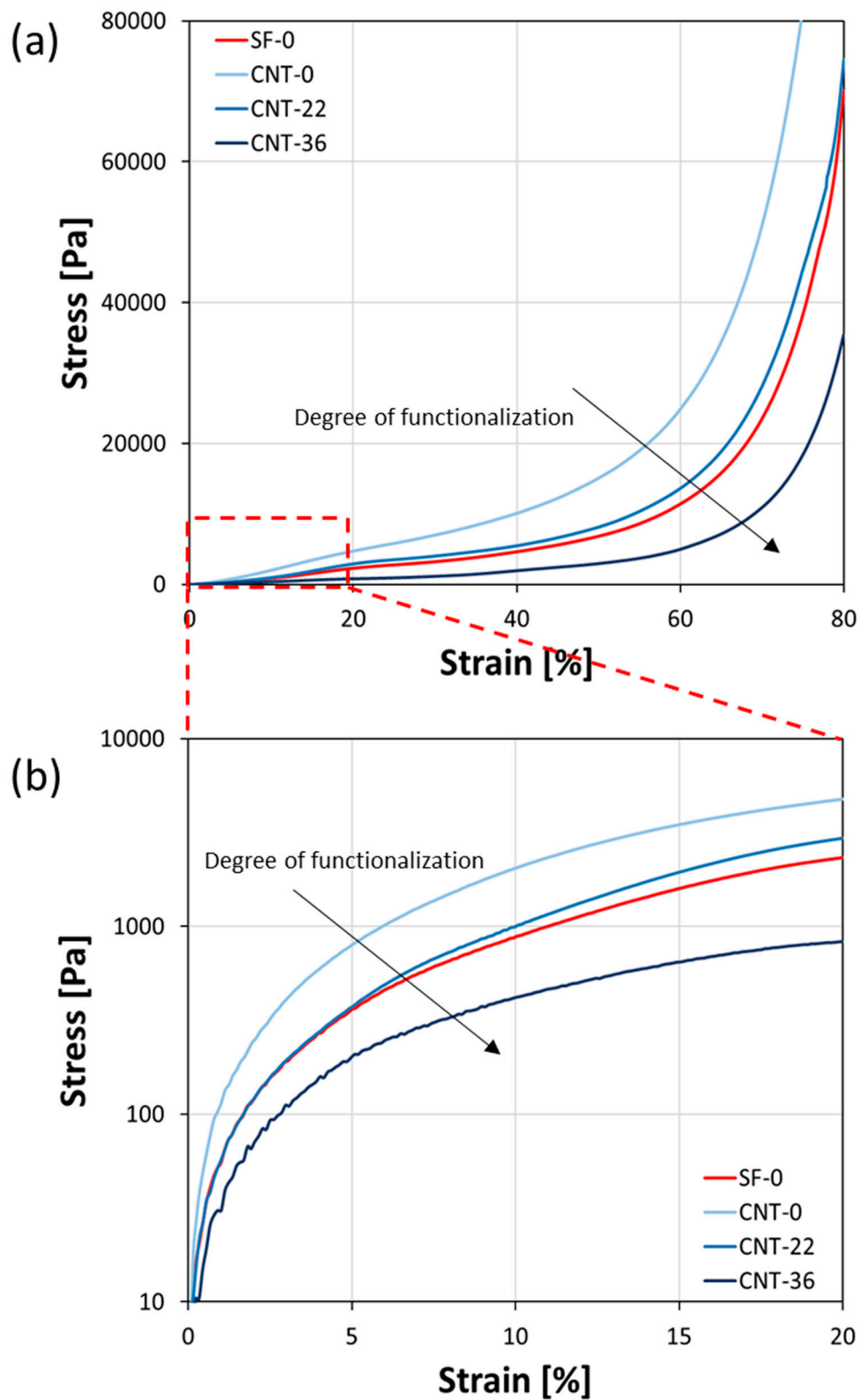


Figure 7. Stress–strain curves of composite foams (a), magnification of up to 20% strain (b).

In fact, the buckling stress is significantly influenced by the foam morphological and physical properties. The foam density is, as expected, strictly correlated with the foam morphology. When the apparent density is low (CNT-22 and CNT-36), foam’s porosity increases, thinning the foam walls; thus, a low buckling stress is observed. If the foaming ratio is lower (CNT-0), the average distance

among the bubbles increases. Therefore, the bubble walls become thicker and the stress value in the plateau region is high [33]. For the CNT-0 composite foam, the collapse regime takes place at a high stress level. In fact, this foam exhibits the highest density (0.315 g/cm^3) and the pore size is small (about 1.05 mm). Thus, a short and a high stress level plateau stage characterizes the material response, because of the densification phase triggering (due to the cell wall contact during the compressive load) at low deformation values.

On the contrary, as quantified in Table 2, functionalized CNT-filled foams exhibit a lower density (0.253 g/cm^3 and 0.251 g/cm^3 , respectively, for CNT-22 and CNT-36) and a consequent larger pore size (1.82 and 2.00 mm, respectively, for CNT-22 and CNT-36). Hence, the densification phase will start at higher deformation values and the plateau extends between a larger deformation range (almost 20–65% for CNT-36) and a lower stress value (0.0008–0.0062 MPa). Furthermore, the densification region is strictly dependent on the foam density. This is confirmed by the densification strain trend. Densification is obtained when the compressive stress closes the foam bubbles and the contact of cell walls occurs. Therefore, a high foaming ratio induces a higher densification strain [33]. Table 2 summarizes the main average compressive parameters acquired from the compression tests for all the composite foams. CNT-0 shows the lowest densification strain (68%); on the contrary, less dense foams exhibit higher values—in particular, CNT-36, whose density is 0.251 g/cm^3 and who reports a 70.21% densification strain.

By the addition of the CNT filler, an increase in the elastic modulus and collapse stress is detected. CNT-0 evidences an elastic modulus of 0.030 MPa, 1.7 times higher than the SF-0 one, and a collapse stress of 0.010 MPa, one order of magnitude higher than the SF-0 sample. While the CNT-22 values appear similar to the ones of mere silicone foam, on the contrary a decrease is detected for the CNT-36 sample, whose elastic modulus is one order of magnitude lower (0.006 MPa) than the unfilled foam's one, and the collapse stress is about 0.002 MPa. The converse consideration can be made for the densification strain. The higher the elastic modulus (0.030 MPa), the lower the densification strain (68%). This trend is related to foam cell wall structure, considering that their collapse stress and elastic modulus increases as the cell wall thickness increases [39].

A further feature that can be assessed by CNT-filled silicone foams is the stress absorption capability. As previously described, oil recovery materials must have the ability to be reused. This advantage extends the material's useful life, lowers the disposal costs, and increases its efficiency. The more the material can be reused, the higher is its added value [20].

Actual sorbent materials used for oil recovery applications usually have a single use before being disposed of [11], reducing their service life. An absorbent material reusable for several cycles of "polluting oil recovery–compression of the absorbent material–emptying and regeneration of it" is suitable. In this regard, both suitable elastic and damping properties are required for an absorbent material to safeguard the risk of mechanical cracking triggering [33] during the compression phase, carried out to empty the material from the absorbed oil and consequently to regenerate it for a further subsequent oil recovery phase.

For engineering tailoring the absorbent foamed materials to this purpose, compressive energy absorption (identifiable as the area subtended by the stress strain curves reported in Figure 7) can be recognized as an indirectly valuable parameter. The compressive absorption energy capacity (EC) is the absorbed energy per volume unit when the composite structure is deformed by compression. It can be defined as the area under the compressive stress–strain curve [40]. EC can be calculated by Equation (2).

$$EC = \int_0^{\epsilon} \sigma d\epsilon, \quad (2)$$

where EC is energy absorption capability and σ and ϵ are stress and strain, respectively.

The evolution of energy absorption capacity (EC) determined based on Equation (2) for all foam batches is presented in Figure 8. It can be observed that the EC parameter gradually increases as the compressive strain increases. Nonetheless, visible changes in absorption energy trend are detected in

the investigated samples, in particular in the CNT-0 and CNT-36 samples, which mostly deviate from the unfilled sample reference, and from the CNT-22 sample, which exhibits a very similar behavior. The cumulative energy absorption capacity of the CNT-0 and CNT-36 batches are, respectively, about 5150 and 1000 J/m³ at a strain of 60%. The difference between the two foams is relevant, indicating that the functionalization degree plays a significant role in the energy absorption capacity. This behavior could be ascribed to the decrease in both cell wall thickness and composite foam density using 36 wt.% functionalized CNT. Thus, if the CNT used as fillers in silicone foam are functionalized, a densification zone is reached at high strains and a higher stress is required in order to dissipate the same energy of other batches [35].

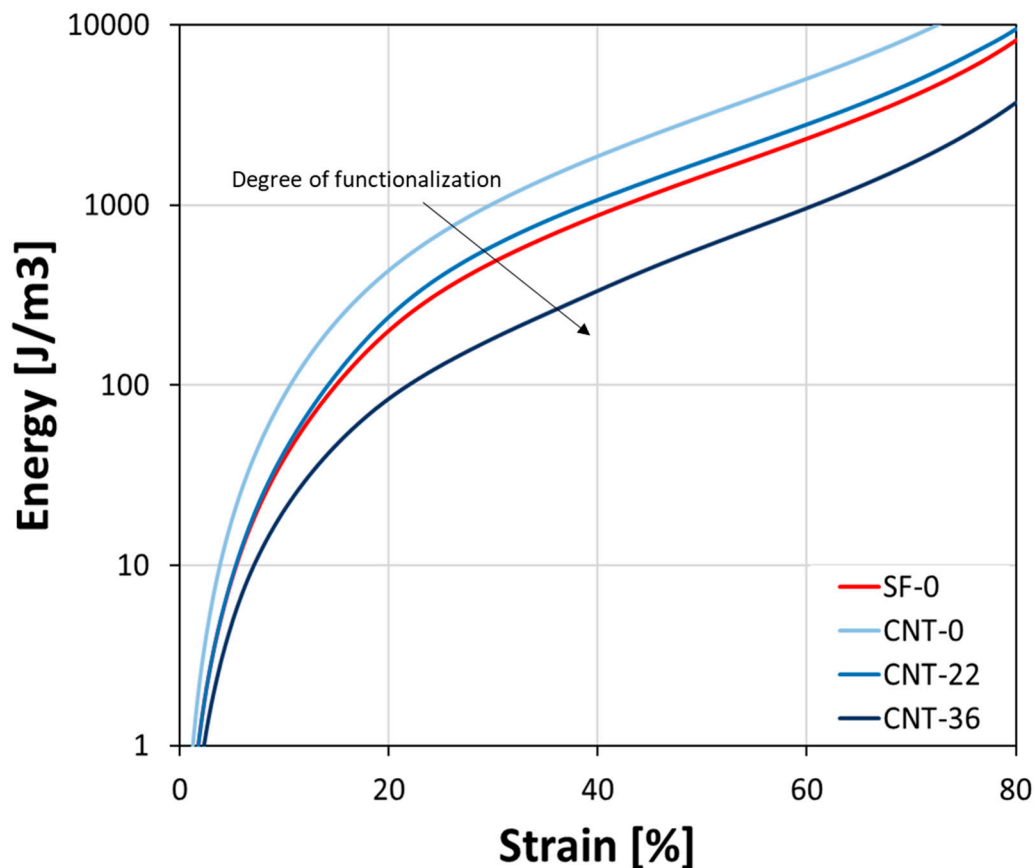


Figure 8. Compressive energy plot of composite foams.

3.4. Cyclic Compression Test

The mechanical stability of the composite material during compressive loading/unloading cycles has been assessed by a cyclic compression test carried out on all batches for up to 30 cycles. In Figure 9, the compressive stress–strain curve of a complete cycle for each studied foam is represented. Using CNT filler in a silicone matrix, an increase in the maximum stress is observed, correlated with a higher absorption energy, described by the hysteresis area under the stress–strain curve. CNT-22 shows the same maximum stress as the SF-0 sample, even if the hysteresis still retains the influence of the CNT presence and appears wider. Increasing the degree of functionalization, the maximum stress significantly decreases and the hysteresis almost flattens down.

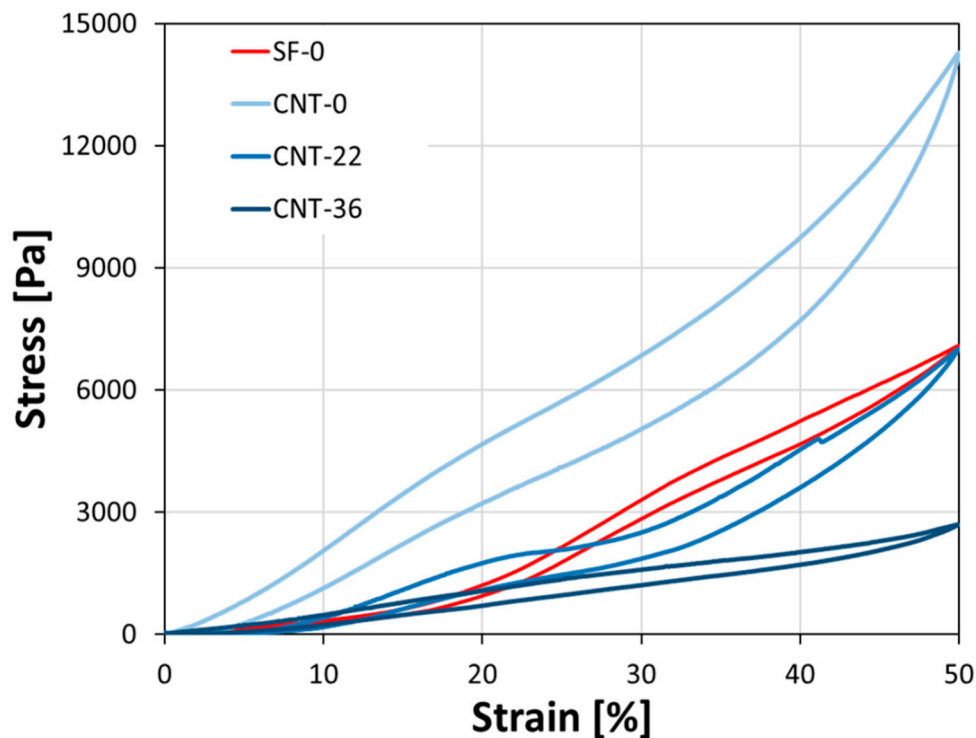


Figure 9. Stress–strain curves for composite foams during one cycle at an ε_{\max} of 50%.

This behavior is likely influenced by the not regular and inhomogeneously large cell size, which affects the foam stability [41].

Figure 10 shows the maximum stress at an increasing number of cycles. For all the investigated foams, the maximum stress decreases as the number of cycles increases, maintaining a strain value fixed at 50%. Two zones can be identified in the obtained curves:

- an unstable zone, where the stress curve exhibits a negative slope and its value decreases as the number of cycles increases from the maximum static stress σ_{stat} (at a zero number of cycles) up to σ_0 (calculated at a number of cycles at which it remains approximately constant);
- a stabilized zone where the stress remains constant at the value of σ_0 almost regardless of the number of cycles.

The transition between the first and second part of the curve occurs at a low number of cycles and is related to the foam rubber-like mechanical behavior. In fact, in the first part of the curve a plastic deformation component is generated due to the foam fatigue caused by the repeated stresses, which reduces the maximum stress tolerated by the foam. This stress decrease, called the Mullins effect or stress softening, is a particular phenomenon typical of filled elastomeric materials whose mechanical response depends on the maximum loading previously encountered [42].

The Mullins effect is also influenced by the interactions between the silicone matrix and filler.

For the silicone foam SF-0, the maximum stress gradually decreases, reaching a plateau at almost 6920 Pa at the 20th cycle. Using CNT as fillers, the composite shows a slower decay of the mechanical properties. The plateau becomes less evident after 30 cycles, when a 13,750 Pa maximum stress is achieved. A particular behavior is observed for the CNT-22 sample, in which a decrease in the maximum stress at low cycles and a further continuous decrease after the 20th cycle are found. This is probably due to the sample's poor morphological homogeneity.

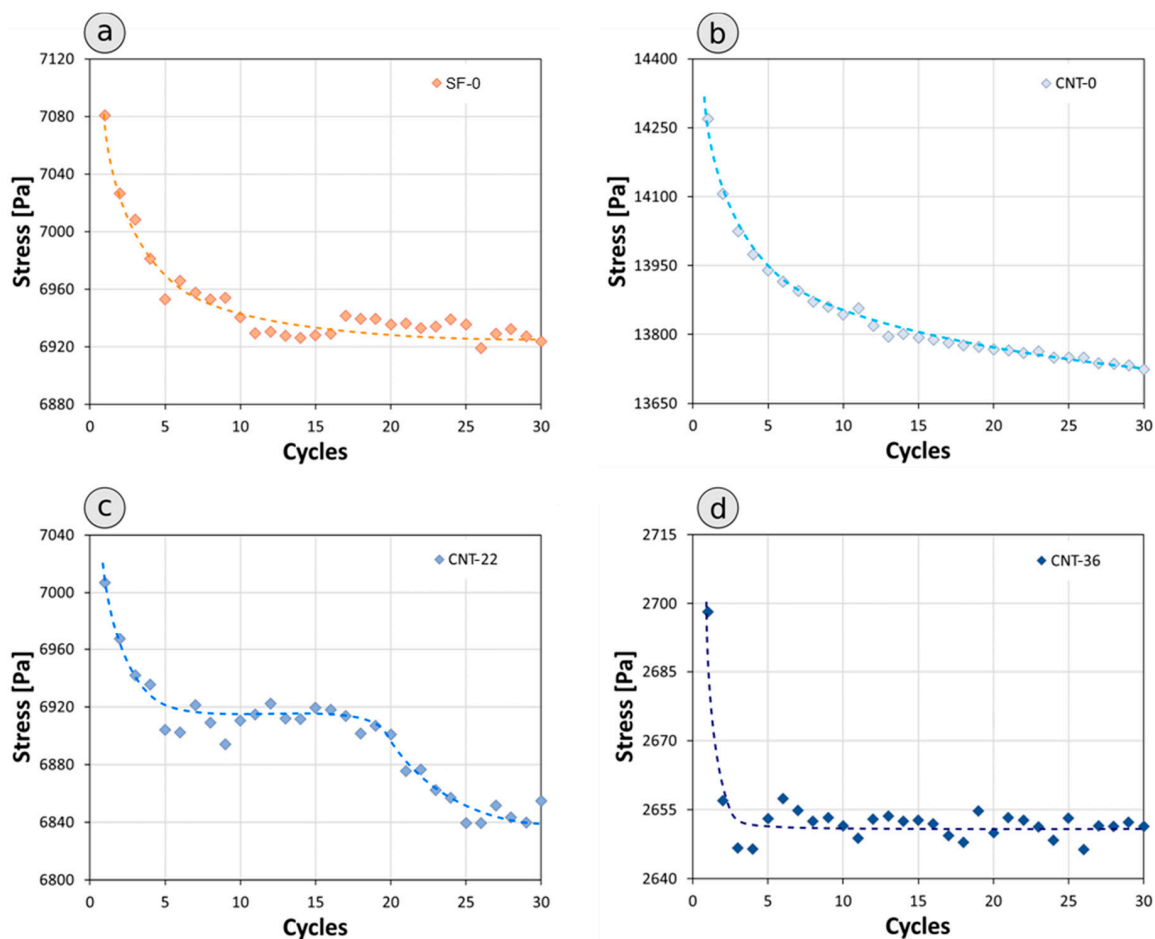


Figure 10. Maximum stress of (a) SF-0, (b) CNT-0, (c) CNT-22, and (d) CNT-36 at an increasing number of cycles ($50\% \epsilon_{\max}$).

The larger pores collapse at low cycles, decreasing the foam elasticity (Figure 11a–c); on the contrary, the small pores with thicker walls promote energy dissipation and retain the foam's compressive strength for a longer time (Figure 11b). The value at the 30th cycle is around 6840 Pa. The performance of the CNT-36 sample, on the contrary, is completely different. The maximum stress undergoes a sudden drop already in the second cycle, reaching a plateau of 2650 Pa in the third cycle. CNT-36 foam, as shown above, is characterized by large pores and presents microcracks in the siloxane matrix (Figure 5) which irreparably, already at the second cycle, weaken the structure, thus permanently compromising its mechanical compressive strength (Figure 11d). As evidenced by the results, the CNT-0 sample, even after 30 cycles, shows the best mechanical performances. Even if, after cycling, microcracks are present also in CNT-0 (Figure 11b), in this case they are not as accentuated as in the SF-0, CNT-22, and CNT-36 samples, where they appear more pronounced and larger (Figure 11a,c,d). Using functionalized CNT, the mechanical properties of the composite material worsen, reaching values close to the unfilled siloxane for the CNT-22 sample and even lower for CNT-36.

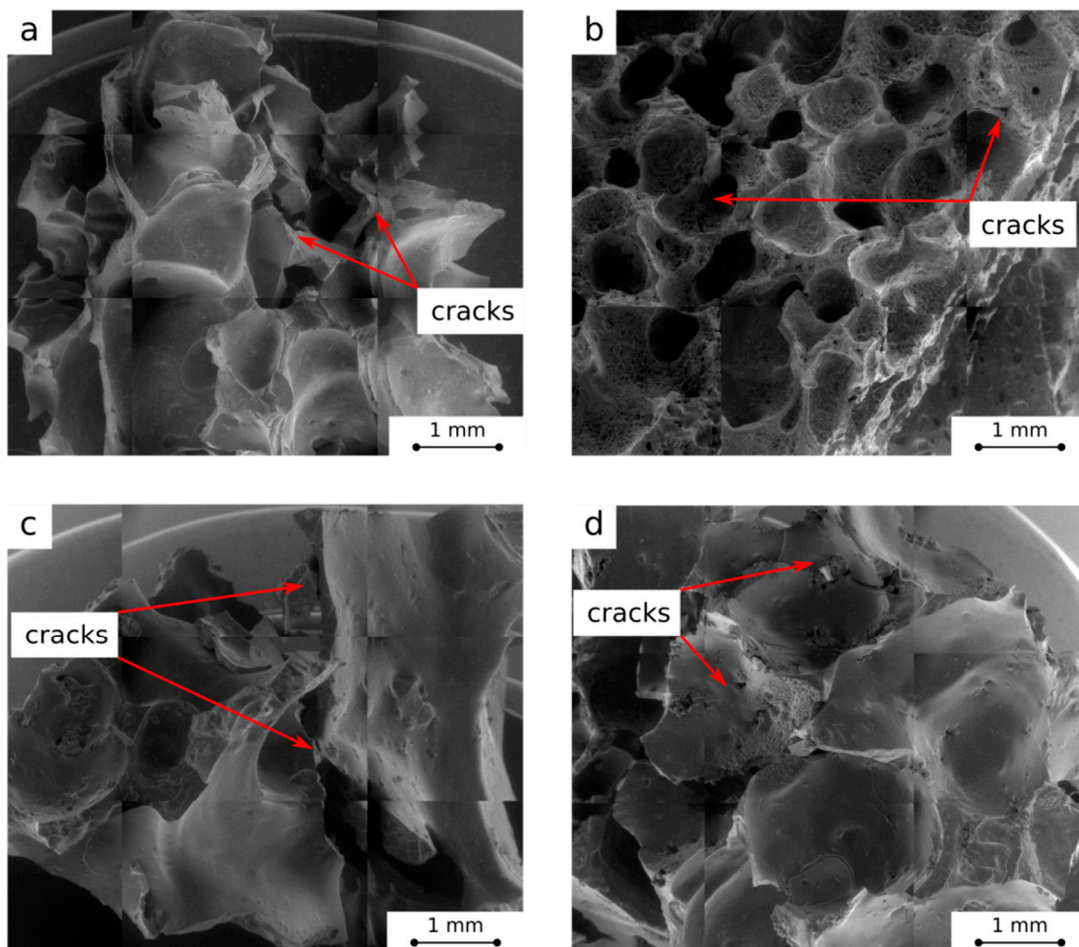


Figure 11. SEM micrographs after kerosene absorption of (a) SF-0, (b) CNT-0, (c) CNT-22, and (d) CNT-36.

A correlation between the morphology, absorption properties, and durability of the composite is crucial to understand the key parameters able to optimize the new material's performance in the desired application.

In Figure 12, a correlation between the absorption capacity, elastic modulus, and foam cyclability is represented. Three zones are recognizable: stable, instable, and high-efficiency zone.

- **Stable zone:** This zone is characterized by a low absorption and high cyclability. In fact, the low percentage of absorption, as previously described, implies a lower volumetric expansion of the foam, which retains its mechanical properties for long time. This behavior is typical of pump oil and crude oil absorption. A good cyclability is maintained also at a high elastic modulus.
- **Unstable zone:** On the contrary, a foam that absorbs a high percentage of polluting oil, such as naphtha and kerosene, is subjected to a considerable increase in volume which greatly stresses the structure, penalizing its mechanical performance. This is described in the unstable area, which reports a minimum at almost 0.017 MPa and 119 wt.% of absorption. The presence of the minimum can be associated with two mechanisms that compete to influence the foam stability or mechanical instability. A foam with a low elastic modulus, as highlighted above, is characterized by easier deformability, thus allowing better mechanical stability following a significant increase in volume. However, a low modulus is also associated with a low breaking stress. Only foams with greater stiffness are also characterized by high resistance to allow an effective mechanical stability even at high absorption. In fact, the instability region comprises high absorption values in a range of elastic modulus up to about 0.0275 MPa. The minimum point identifies a foam

characterized by a sufficiently elastic morphology but not sufficiently resistant to withstand the effort imposed by the increase in volume.

- High efficiency zone: This zone is, instead, characterized by a high elastic modulus and high absorption values. In such a context, when increasing the elastic modulus the composite stiffness increases, but at the same time also the maximum compression stress value rises, ensuring a longer material cyclability.

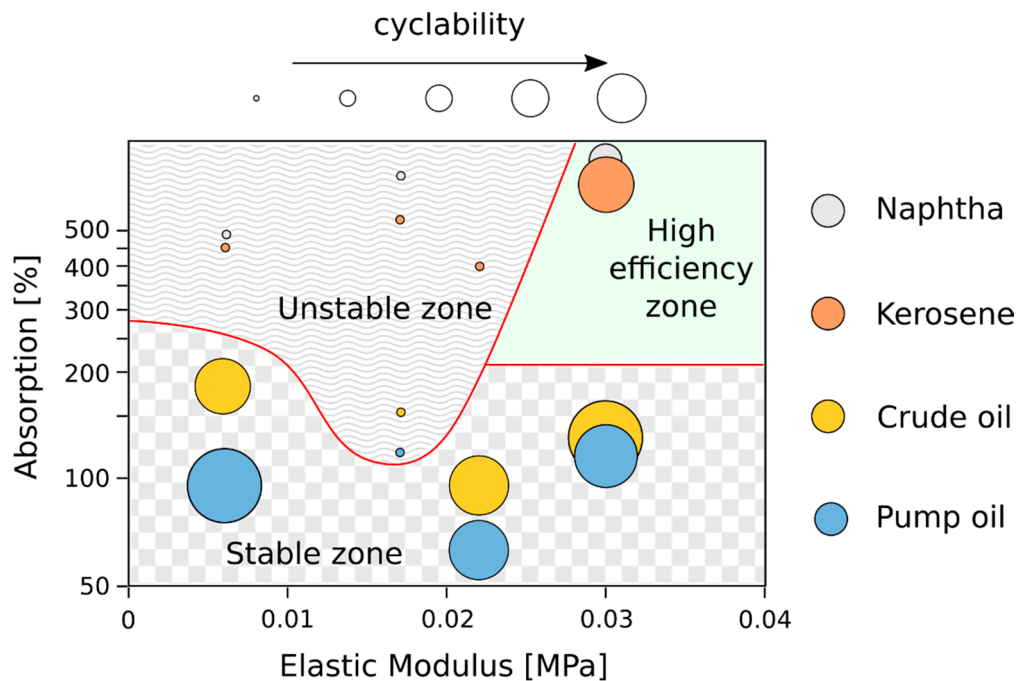


Figure 12. Correlation between the absorption capacity (%), elastic modulus (MPa), and cyclability.

As highlighted in Figure 7, all the batches exhibited a quite relevant compressibility, indicating a suitable foam flexibility also for a high elastic modulus. However, their absorption capacity and cyclability property are different (Figure 12). Depending on the absorption properties, foams with a very low stiffness (CNT-36 batch) can exhibit an unstable mechanical cyclability. The macroporus structure leads to a soft mechanical behavior, characterized by very large flexibility and high densification strain. This allows it to have an acceptable cyclability in pump oil and crude oil, where a low pollutant absorption occurs. When the absorption performances are high, as in light oil (kerosene and naphtha) the durability decreases significantly because the material is not mechanically suitable to suffer the generated stress during the foam expansion. An increase in stiffness at intermediate elastic modulus values (SF-0 and CNT-22 batches, with an $E_{SF-0} = 0.017$ MPa and $E_{CNT-22} = 0.022$ MPa, respectively) is detrimental to the material durability under absorption cycles. In particular, the SF-0 batch shows the lowest cyclability both in heavy and light oils. These foams suffer a mechanical instability during cycles in either light or heavy oils. The foams' morphological characteristics, indeed, do not allow a good resistance to repeated "absorption-squeezing" cycles. On the contrary, composite foam with a high elastic modulus (CNT-0 batch) has a relevant oil absorption capacity and can be squeezed many times. Furthermore, an effective cyclability takes place. The combined action of these properties allows one to obtain a more sustainable material for oil recovery applications.

According to this stability map (Figure 12), CNT-silicone composite foam must be designed with an elastic modulus higher than 0.03 MPa in order to guarantee the adequate mechanical resistance to bear the stresses induced by the absorption of oil pollutants. The elastic and mechanically soft nature of the silicone matrix prevents the formation of a hard and brittle material which would prejudice cycling properties. These results are fundamental for a proper design of foams that can combine morphology

with long-term performance and a high absorption capacity. At this aim, this work is intended to be a simplified approach for tailoring a long-lasting absorption performance of CNT-filled silicone foams.

In light of these promising results, we are confident that a well-defined design of the absorbing material at macro- and microstructural level will provide the opportunity to overcome the actual issues for long-lasting economic approaches in oil recovery application processes [8,43]. Indeed, a continuous effort devoted to improving the knowledge in the applied research and potential industrialization of the absorbent composite materials will be applied for water remediation in the following years [11]. In addition, the notable advantage of the easy scalability of the proposed manufacturing process furthermore encourages the use of this class of composite macroporous structures for achieving higher efficiencies in oil/water separation and collection processes [23,44]. Nevertheless, further research efforts are required to effectively and efficiently address global water pollution from oil spills and organic pollutants. In this regard, the targeted design of materials is a particularly useful approach for future developments and innovations in the sector [25].

4. Conclusions

The mechanical behavior under different compression loads of an innovative oil recovery foam was investigated. The composite material was realized by the introduction of CNT fillers in a silicone matrix. Pristine and functionalized CNT were used as fillers and an unfilled silicone foam (SF-0) was studied as a reference material. The obtained products were characterized morphologically and mechanically. The absorption properties in kerosene, naphtha, pump oil, and crude oil, as previously investigated in already published works, were correlated with mechanical performances and physical characteristics, such as density and pore size. The mechanical investigation was performed by static and cyclic compression tests. The use of CNT as a filler (CNT-0 sample) significantly increases the mechanical properties of the silicone matrix, improving the material compression strength. In fact, an increase in the materials' Young's modulus (0.030 MPa) and collapse stress (0.010 MPa) was observed. Meanwhile, the use of functionalized CNT worsens the mechanical characteristics. This behavior was confirmed in cyclic tests. In fact, the CNT-0 sample continues to maintain its excellent mechanical properties even at the 30th cycle. This entails the material reuse that translates into a considerable economic and environmental advantage. On the contrary, samples filled with functionalized CNT undergo to a decrease in compression stress below the unfilled silicone foam, specifically employing CNT fillers at the highest degree of functionalization (2650 Pa and 6920 Pa for CNT-36 and SF-0, respectively). This is probably due to the morphological characteristics of these foams, characterized by a lower density due to the presence of large and inhomogeneous pores and microfractures. Furthermore, a close correlation between the mechanical behavior, absorption capacity, and cyclability was verified. The higher the degree of absorption, the lower the foam's cyclability, as the considerable increase in volume subjects the foam to mechanical stress, which leads to its decay. Meanwhile, at low absorption the cyclability increases. A high efficiency level is achieved at high absorptions and a high Young's modulus because of the simultaneous increase in the foam's stiffness and maximum compression stress, thus allowing the repeated use of the composite material for numerous cycles.

Author Contributions: Conceptualization, C.M.; Data curation, L.C.; Formal analysis, E.P. (Elpida Piperopoulos), L.C. and E.M.; Investigation, E.P. (Elpida Piperopoulos); Methodology, E.P. (Elpida Piperopoulos) and L.C.; Supervision, E.P. (Edoardo Proverbio); Validation, E.P. (Edoardo Proverbio) and C.M.; Writing—original draft, E.P. (Elpida Piperopoulos), L.C. and E.M.; Writing—review and editing, E.P. (Edoardo Proverbio) and C.M. All authors have read and agreed to the published version of the manuscript.

Funding: This research received no external funding.

Conflicts of Interest: The authors declare no conflict of interest.

References

1. ISPRA. *Quaderni Delle Emergenze Ambientali in Mare*; Istituto Superiore per la Protezione e la Ricerca Ambientale (ISPRA): Roma, Italy, 2014; pp. 1–9.
2. Hatzianestis, I.; Parinos, C.; Bouloubassi, I.; Gogou, A. Polycyclic aromatic hydrocarbons in surface sediments of the Aegean Sea (eastern Mediterranean Sea). *Mar. Pollut. Bull.* **2020**, *153*, 111030. [[CrossRef](#)]
3. Sepp Neves, A.A.; Pinardi, N.; Navarra, A.; Trotta, F. A General Methodology for Beached Oil Spill Hazard Mapping. *Front. Mar. Sci.* **2020**, *7*, 1–10. [[CrossRef](#)]
4. Kukkar, D.; Rani, A.; Kumar, V.; Younis, S.A.; Zhang, M.; Lee, S.S.; Tsang, D.C.W.; Kim, K.H. Recent advances in carbon nanotube sponge-based sorption technologies for mitigation of marine oil spills. *J. Colloid Interface Sci.* **2020**, *570*, 411–422. [[CrossRef](#)] [[PubMed](#)]
5. Brussaard, C.P.D.; Peperzak, L.; Beggah, S.; Wick, L.Y.; Wuerz, B.; Weber, J.; Samuel Arey, J.; Van Der Burg, B.; Jonas, A.; Huisman, J.; et al. Immediate ecotoxicological effects of short-lived oil spills on marine biota. *Nat. Commun.* **2016**, *7*, 11206–11216. [[CrossRef](#)]
6. Beyer, J.; Trannum, H.C.; Bakke, T.; Hodson, P.V.; Collier, T.K. Environmental effects of the Deepwater Horizon oil spill: A review. *Mar. Pollut. Bull.* **2016**, *110*, 28–51. [[CrossRef](#)] [[PubMed](#)]
7. Freitas, B.G.; Brito, J.G.M.; Brasileiro, P.P.F.; Rufino, R.D.; Luna, J.M.; Santos, V.A.; Sarubbo, L.A. Formulation of a commercial biosurfactant for application as a dispersant of petroleum and by-products spilled in oceans. *Front. Microbiol.* **2016**, *7*, 1–9. [[CrossRef](#)]
8. Tuan Hoang, A.; Viet Pham, V.; Nam Nguyen, D. A Report of Oil Spill Recovery Technologies. *Int. J. Appl. Eng. Res.* **2018**, *13*, 4915–4928.
9. Doshi, B.; Sillanpää, M.; Kalliola, S. A review of bio-based materials for oil spill treatment. *Water Res.* **2018**, *135*, 262–277. [[CrossRef](#)]
10. Gupta, S.; Tai, N.H. Carbon materials as oil sorbents: A review on the synthesis and performance. *J. Mater. Chem. A* **2016**, *4*, 1550–1565. [[CrossRef](#)]
11. Bhardwaj, N.; Bhaskarwar, A.N. A review on sorbent devices for oil-spill control. *Environ. Pollut.* **2018**, *243*, 1758–1771. [[CrossRef](#)]
12. Al-Jammal, N.; Yuzhakova, T. Review of the Effectiveness of Absorbent Materials in Oil. In Proceedings of the 7th International Conference of ICEEE, Budapest, Hungary, 2017; pp. 131–138.
13. El-Mekawy, A.M.; Mohammed, A.M.F.; Hassan, S.K.M. A review of airborne polycyclic aromatic hydrocarbons (PAHs) and their. *Egypt. J. Environ. Res.* **2016**, *25*, 107–123.
14. Zhou, W.; Xin, C.; Chen, S.; Yu, Q.; Wang, K. Polymer-Enhanced Foam Flooding for Improving Heavy Oil Recovery in Thin Reservoirs. *Energy Fuels* **2020**, *34*, 4116–4128. [[CrossRef](#)]
15. Latif, W.M.S.M.; Sharbini, S.N.; Wan Sulaiman, W.R.; Idris, A.K. Utilization of silicon dioxide nanoparticles in foam enhanced oil recovery—A comprehensive review. *IOP Conf. Ser. Mater. Sci. Eng.* **2019**, *469*, 012027–012036. [[CrossRef](#)]
16. Tang, J.; Vincent-Bonnieu, S.; Rossen, W.R. CT core flood study of foam flow for enhanced oil recovery: The effect of oil type and saturation. *Energy* **2019**, *188*, 116022–116032. [[CrossRef](#)]
17. Ko, T.J.; Hwang, J.H.; Davis, D.; Shawkat, M.S.; Han, S.S.; Rodriguez, K.L.; Oh, K.H.; Lee, W.H.; Jung, Y. Superhydrophobic MoS₂-based multifunctional sponge for recovery and detection of spilled oil. *Curr. Appl. Phys.* **2020**, *20*, 344–351. [[CrossRef](#)]
18. Wang, N.; Deng, Z. Synthesis of magnetic, durable and superhydrophobic carbon sponges for oil/water separation. *Mater. Res. Bull.* **2019**, *115*, 19–26. [[CrossRef](#)]
19. Li, Z.T.; Lin, B.; Jiang, L.W.; Lin, E.C.; Chen, J.; Zhang, S.J.; Tang, Y.W.; He, F.A.; Li, D.H. Effective preparation of magnetic superhydrophobic Fe₃O₄/PU sponge for oil-water separation. *Appl. Surf. Sci.* **2018**, *427*, 56–64. [[CrossRef](#)]
20. Yuan, J.; Zhang, M.; Xia, M.; Cao, W.; Du, M.; Dou, J.; Zhao, D. Novel high-capacity and reusable carbonaceous sponges for efficient absorption and recovery of oil from water. *Appl. Surf. Sci.* **2019**, *487*, 398–408. [[CrossRef](#)]
21. Ding, L.; Li, Y.; Jia, D.; Deng, J.; Yang, W. β -Cyclodextrin-based oil-absorbents: Preparation, high oil absorbency and reusability. *Carbohydr. Polym.* **2011**, *83*, 1990–1996. [[CrossRef](#)]
22. Korhonen, J.T.; Kettunen, M.; Ras, R.H.A.; Ikkala, O. Hydrophobic nanocellulose aerogels as floating, sustainable, reusable, and recyclable oil absorbents. *ACS Appl. Mater. Interfaces* **2011**, *3*, 1813–1816. [[CrossRef](#)]

23. Piperopoulos, E.; Calabrese, L.; Mastronardo, E.; Proverbio, E.; Milone, C. Synthesis of reusable silicone foam containing carbon nanotubes for oil spill remediation. *J. Appl. Polym. Sci.* **2018**, *135*, 46067–46078. [[CrossRef](#)]
24. Piperopoulos, E.; Calabrese, L.; Mastronardo, E.; Abdul Rahim, S.H.; Proverbio, E.; Milone, C. Assessment of sorption kinetics of carbon nanotube-based composite foams for oil recovery application. *J. Appl. Polym. Sci.* **2019**, *136*, 47374–47387. [[CrossRef](#)]
25. Ge, M.; Cao, C.; Huang, J.; Zhang, X.; Tang, Y.; Zhou, X.; Zhang, K.; Chen, Z.; Lai, Y. Rational design of materials interface at nanoscale towards intelligent oil-water separation. *Nanoscale Horiz.* **2018**, *3*, 235–260. [[CrossRef](#)] [[PubMed](#)]
26. Messina, G.; Modafferi, V.; Santangelo, S.; Tripodi, P.; Donato, M.G.; Lanza, M.; Galvagno, S.; Milone, C.; Piperopoulos, E.; Pistone, A. Large-scale production of high-quality multi-walled carbon nanotubes: Role of precursor gas and of Fe-catalyst support. *Diam. Relat. Mater.* **2008**, *17*, 1482–1488. [[CrossRef](#)]
27. Santangelo, S.; Piperopoulos, E.; Fazio, E.; Faggio, G.; Ansari, S.; Lanza, M.; Neri, F.; Messina, G.; Milone, C. A safer and flexible method for the oxygen functionalization of carbon nanotubes by nitric acid vapors. *Appl. Surf. Sci.* **2014**, *303*. [[CrossRef](#)]
28. Calabrese, L.; Bonaccorsi, L.; Freni, A.; Proverbio, E. Synthesis of SAPO-34 zeolite filled macrocellular foams for adsorption heat pump applications: A preliminary study. *Appl. Therm. Eng.* **2017**, *124*, 1312–1318. [[CrossRef](#)]
29. Piperopoulos, E.; Calabrese, L.; Khaskhoussi, A.; Proverbio, E.; Milone, C. Thermo-physical characterization of carbon nanotube composite foam for oil recovery applications. *Nanomaterials* **2020**, *10*, 86–102. [[CrossRef](#)] [[PubMed](#)]
30. Fiore, V.; Piperopoulos, E.; Calabrese, L. Assessment of Arundo donax fibers for oil spill recovery applications. *Fibers* **2019**, *7*, 75. [[CrossRef](#)]
31. Calabrese, L.; Bonaccorsi, L.; Bruzzaniti, P.; Freni, A.; Proverbio, E. Morphological and functional aspects of zeolite filled siloxane composite foams. *J. Appl. Polym. Sci.* **2018**, *135*, 1–10. [[CrossRef](#)]
32. ASTM. E111-04 Young's Modulus, Tangent Modulus, and Chord Modulus 1. *Stand. Test. Method ASTM Int.* **2010**, 1–7.
33. Calabrese, L.; Bonaccorsi, L.; Bruzzaniti, P.; Gulli, G.; Freni, A.; Proverbio, E. Zeolite filled siloxane composite foams: Compression property. *J. Appl. Polym. Sci.* **2018**, *135*, 46145–46155. [[CrossRef](#)]
34. Elliott, J.A.; Windle, A.H.; Hobdell, J.R.; Eeckhaut, G.; Oldman, R.J.; Ludwig, W.; Boller, E.; Cloetens, P.; Baruchel, J. In-situ deformation of an open-cell flexible polyurethane foam characterised by 3D computed microtomography. *J. Mater. Sci.* **2002**, *37*, 1547–1555. [[CrossRef](#)]
35. Gibson, L.J.; Ashby, M.F. *Cellular Solids: Structure and Properties*, 2nd ed.; Cambridge University Press: Cambridge, UK, 2014; ISBN 9781139878326.
36. Duarte, I.; Ferreira, J.M.F. Composite and nanocomposite metal foams. *Materials* **2016**, *9*, 79. [[CrossRef](#)]
37. Avalle, M.; Belingardi, G.; Montanini, R. Characterization of polymeric structural foams under compressive impact loading by means of energy-absorption diagram. *Int. J. Impact Eng.* **2001**, *25*, 455–472. [[CrossRef](#)]
38. Bouix, R.; Viot, P.; Lataillade, J.L. Polypropylene foam behaviour under dynamic loadings: Strain rate, density and microstructure effects. *Int. J. Impact Eng.* **2009**, *36*, 329–342. [[CrossRef](#)]
39. Yu, H.; Guo, Z.; Li, B.; Yao, G.; Luo, H.; Liu, Y. Research into the effect of cell diameter of aluminum foam on its compressive and energy absorption properties. *Mater. Sci. Eng. A* **2007**, *454–455*, 542–546. [[CrossRef](#)]
40. Baumeister, J.; Banhart, J.; Weber, M. Aluminium foams for transport industry. *Mater. Des.* **1997**, *18*, 217–220. [[CrossRef](#)]
41. Gong, L.; Kyriakides, S.; Jang, W.Y. Compressive response of open-cell foams. Part I: Morphology and elastic properties. *Int. J. Solids Struct.* **2005**, *42*, 1355–1379. [[CrossRef](#)]
42. Pan, Y.; Zhong, Z. Modeling the Mullins effect of rubber-like materials. *Int. J. Damage Mech.* **2017**, *26*, 933–948. [[CrossRef](#)]
43. Scott, A.J.; Penlidis, A. Designing Optimal Terpolymers for Enhanced Oil Recovery (Polymer Flooding). *Ind. Eng. Chem. Res.* **2020**, *59*, 7426–7437. [[CrossRef](#)]
44. Zhang, N.; Zhong, S.; Zhou, X.; Jiang, W.; Wang, T.; Fu, J. Superhydrophobic P (St-DVB) foam prepared by the high internal phase emulsion technique for oil spill recovery. *Chem. Eng. J.* **2016**, *298*, 117–124. [[CrossRef](#)]

